[Frontiers in Bioscience, Elite, 5, 517-524, January 1, 2013]

Real-time imaging of mouse lenticulostriate artery following brain ischemia

Falei Yuan[1], Yongting Wang[1], Yongjing Guan[1, 2], Yuqi Ren[3], Haiyan Lu[1], Tiqiao Xiao[3], Honglan Xie[3], Peter S. Vosler[4], Jun Chen[4], Guo-Yuan Yang[1, 2]

[1]Neuroscience and Neuroengineering Research Center, Med-X Research Institute, School of Biomedical Engineering, Shanghai Jiao Tong University, Shanghai, China, [2]Ruijin Hospital, School of Medicine, Shanghai Jiao Tong University, Shanghai 200030, China, [3]Shanghai Institute of Applied Physics, Chinese Academy of Sciences, Shanghai, China, [4]Department of Neurology and Pharmacology, University of Pittsburgh, Pittsburgh, PA 15213, USA

TABLE OF CONTENTS

1. ABSTRACT

Detection of microvascular changes in experimental stroke models is limited by current technologies. Using state-of-the-art synchrotron radiation (SR), we explored the feasibility of detecting the normal morphological variations of lenticulostriate arteries (LSAs) and the changes to LSAs following middle cerebral artery occlusion (MCAO). Cerebral microvessels of ICR mice were imaged with synchrotron radiation microangiography using nonionic iodine and barium sulfate as contrast agents. Using SR we reproducibly observed the detailed cerebral microvasculature of LSAs arising from the origin of middle cerebral artery (MCA) with a resolution of approximately 5 micrometers, at least a 20-fold greater resolution compared to CT or MRI imaging. Notably, SR microangiography was able to reveal ischemia/reperfusion induced leakage in the lenticulostriate artery territory. To our knowledge this is the first time that the three-dimensional morphology of LSAs and real time visualization of LSA hemorrhage have been characterized in live mice. This work demonstrates that SR microangiography can provide a unique tool for furthering experimental stroke research to examine the efficacy of neuroprotective therapies on parameters such as angiogenesis and vascular integrity.

2. INTRODUCTION

Growing evidence suggests that the dysfunction of cerebral microvasculature is related to a number of diseases including Alzheimer's disease, vascular dementia, and ischemic and hemorrhagic stroke. This, paired with the growing epidemiological prevalence of diseases such as diabetes and atherosclerosis that cause systemic microvasculature-related alterations, indicates a crucial necessity for the further understanding of how changes in microvasculature contribute to the pathogenesis of the aforementioned disorders (1). Unfortunately the availability of cerebral microvasculature imaging *in vivo* with sufficient resolution is limited by conventional imaging technology.

Current methods of cerebrovascular observation of living animals include optical imaging, CT, MRI, and PET, which are useful tools for understanding the structure and morphology of brain vasculature. The resolution of CT and MRI is approximately 200 micrometers, which is higher than the 1-2 mm resolution of micro-PET. However, this level of resolution does not allow for adequate observation of small vessels (2, 3). To better understand the pathology of cerebrovascular diseases, real time

observation of small morphological changes in the cerebrovasculature is critical.

Synchrotron radiation angiography was developed to meet this challenge (4, 5). The Shanghai Synchrotron Radiation Facility (SSRF) is a newly established third generation SR light source in China (6, 7). It operates with the electron beam energy of 3.5 GeV. As seen with other third generation SR light sources such as ESRF and Spring-8, SR provides a new solution to achieving high-resolution imaging in living animals. Recent developments in SR imaging have allowed the characterization of brain vasculature in living rats (8, 9) and in *ex vivo* mouse brain (10). However, observation of small vessels in living mice has yet to be reported.

Cerebrovascular abnormalities including aneurysms, arteriovenous malformations, and vasospasm are related to both ischemic and hemorrhagic stroke. The majority of hemorrhagic stroke (66.5%) is induced by the rupture of lenticulostriate arteries (LSAs), which are small branches of the MCA that supply blood to the caudate nucleus, putamen, and globus pallidus of striatum (11). This high occurrence can be partially attributed to the special structure of LSAs because they are end arteries that have no collateral blood supply (12). This is clinically relevant because of the increased risk of LSA aneurysms in patients with hypertension (13).

The pathogenesis of lacunar stroke induced by LSA lesion is still poorly understood, and there is a lack of appropriate animal models and imaging tools (14, 15). Clinically, LSAs in humans can be observed by digital subtraction angiography (DSA) (16). Unfortunately, in small animals such as mice, LSAs are too small to be detected with conventional methods. LSAs are believed to have irregular patterns and unique structures. However, little is known about their exact morphology in living mice.

The first cerebral LSA imaging on rats demonstrated that systemic hypotension distended LSAs but constricted most of the large cerebral trunk vessels (9). A similar study observed increased dilatation on LSAs compared to cortical arteries when rat blood pressure was reduced to 40-59 mmHg by arterial bleeding (8). Finally, observation of intracerebral arteries in extracted ischemic mouse brain using barium sulfate as contrast agent demonstrated a dramatic decrease of intracerebral arteries in the ischemic area two days after stroke (10). To date, however, characterization of LSAs in living mice has not been feasible. In this study we report novel use of cerebral SR microangiography in living mice by characterizing the three-dimensional pattern of the cerebral vasculature of LSAs under both normal and ischemic conditions.

3. MATERIALS AND METHODS

3.1. Middle cerebral artery occlusion

Animal procedures for the use of laboratory animals were approved by the Institutional Animal Care and Use Committee of Shanghai Jiao Tong University. The surgical procedure was described previously (17). Ten adult male ICR mice weighing 35-40 grams were used. Mice were anesthetized with 7% chloral hydrate (350 mg/kg) intraperitoneally, and the body temperature was maintained at 37ºC by a heating pad (RWD life science, Shenzhen, China). A midline incision was made on the neck under an operating microscope (Leica, Germany). The left common carotid artery (CCA), the external carotid artery (ECA) and the internal carotid artery (ICA) were isolated. A silicone-coated 6-0 suture was inserted from the ECA stump to the ICA to induce MCAO. The distance from the bifurcation to the ostium of MCA was 9 mm. The suture was withdrawn after 1 hour for reperfusion. Twenty four hours after reperfusion, a PE-10 catheter was carefully inserted from the distal ECA into the ICA/CCA for iodine injection. The occlusion and reperfusion of MCA were verified by a laser doppler flowmetry (Moor Instruments, England).

3.2. SR parameters

The storage ring at SSRF was operated at 3.5 GeV electron beam energy. The average beam current was 180 mA. This synchrotron beam was monochromatized by two pieces of silicon crystal, which were placed in front of the imaging hutch. Considering both the resolution and the region of interest (ROI), CCD cameras with a resolution of 9 micrometer or 13 micrometer (Photonic Science, Britain) were selected in this study. The beamline generates a bundle of hard x-ray with a field of view up to 45 mm (Horizontal) ×5 mm (Vertical). The distance between the point source from the electric storage ring and brain was 34 meters (Figure 1).

3.3. SR imaging

3.3.1 Cerebral angiography *in situ*

Five mice were used in this study. A total volume of 1 mL BaSO4 with average particle diameters of 0.7 micrometer glycerin (50% aqueous solution) suspension was introduced through a PE-10 catheter for each mouse. The mouse was suspended on a bracket that was vertical to the SR beam. The bracket was then placed on an adjustable platform, located 65 cm away from the CCD camera. At least eight images of the cerebrovascular system were taken for each animal. These images were reconstructed to present the vasculature of the whole brain.

3.3.2.Cerebral angiography *in vivo*

Five mice were cannulated as described above, and the cannula was connected to an injection system consisting of a precise injection pump with screen display (Longer pump, China), a five-voltage DC power supply, and a switch. The latter two were used for remote control of the injection pump outside the imaging hutch by changing the electricity level that controlled the injection pump. The injection volume of contrast agent can be read from the screen of the injection pump via a real-time camera inside the hutch.

The mouse was placed perpendicular to the beam on its side. X-ray energy of 33.2 KeV, which is just above the iodine K-edge energy threshold, was used. Nonionic iodine contrast agent (350 mgI/mL, Omnipaque, GE, USA) was injected into the ECA and CCA bifurcation at a rate of

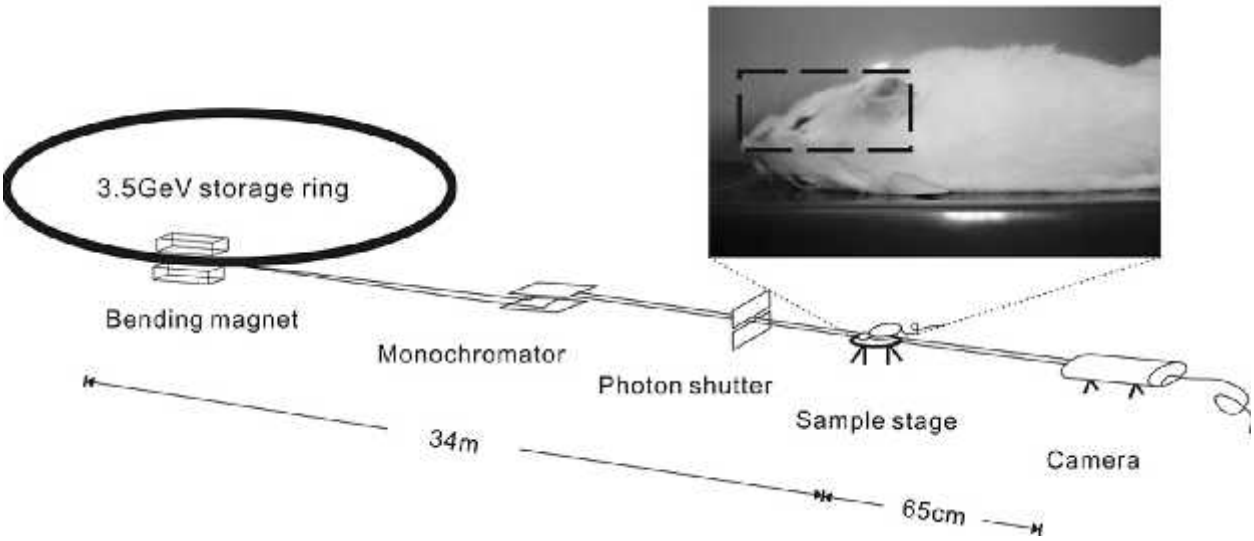

Figure 1. Schematic illustration of synchroton radiation. The X-ray beam emanated from a round electronic storage ring, and projected onto the animal brain after monochromatization by a set of silicon crystal monochromator. The imaging distance is 34 meters from the point-source to animal, and 65 centimeters from the animal to the CCD camera. The picture in the upper right corner shows the position of the mouse, which is perpendicular to the beam. The dashed frame is the area that hard X-rays projected on the mouse brain. Imaging data were collected by a CCD camera.

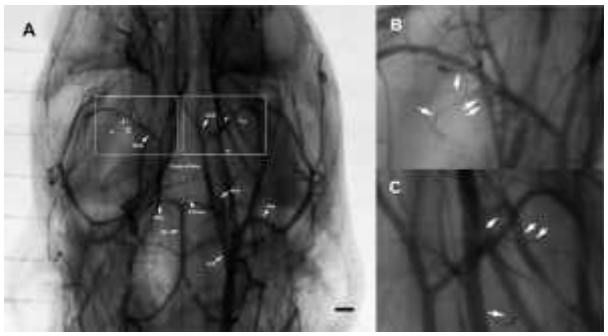

Figure 2. Vasculature of the entire mouse brain. (A) LSAs were observed in both hemispheres of the brain (small arrows) using barium sulfate as the contrast agent. Four LSAs originated from the horizontal segment of left MCA, and four from the right MCA. Other cerebral vessels were clearly shown (large arrows). Images B and C are amplifications of the left and right boxes in A as indicated. LSA, lenticulostriate artery; ACA, anterior cerebral artery; MCA, middle cerebral artery; PCA, posterior cerebral artery; SCA, superior cerebellum artery; BA basilar artery; PcomA, posterior communicating artery; PPA, pterygopalatine artery; and ICA, internal carotid artery. Scale bar = 1 mm.

33.3 microliter/sec for 3 seconds, with a total volume of 100 microliter. The CCD camera was placed 65 cm from the head of animal.

3.4. CT imaging

Immediately after euthanasia, a total volume of 1 mL $BaSO_4$ with average particle diameters of 0.7 micrometer and glycerin (50% aqueous solution) suspension was injected through a PE-10 catheter. Mouse brains were removed after $BaSO_4$ injection. CT images were acquired at 15.8 KeV every 157 ms. A series of 6000 raw images were generated for each brain sample.

3.5. Image processing

Raw data were processed with Image Pro Plus 6.0 (Media Cybernetics Inc., USA) to eliminate background noise produced by CCD camera. The diameters of the vessels were measured using the same software. To present a large-scale view of the brain, the images were combined using Adobe Photoshop CS4 (Adobe Systems Inc. USA). CT slices were generated by a parallel beam filtered back projection reconstruction algorithm written by Interactive Data Language (IDL 7.0). CT reconstruction was performed using Amira 4.1 software (Mercury Computer Systems, USA).

4. RESULTS

4.1. Characteristics of LSAs

Mouse brain microangiography was conducted using barium sulfate. LSAs were observed in the brain bilaterally (Figure 2). Other main branches arising from

Table 1. Diameters of Mouse MCA and LSA

Unit: μm	Mouse_1	Mouse_2	Mouse_3	Mouse_4	Mouse_5	Mean±SD (n=5)
MCA (micrometer)	142.12	166.48	151.61	160.44	135.72	151.27±12.66
LSA (micrometer)	35.51	44.94	39.56	42.22	53.54	43.15±6.77

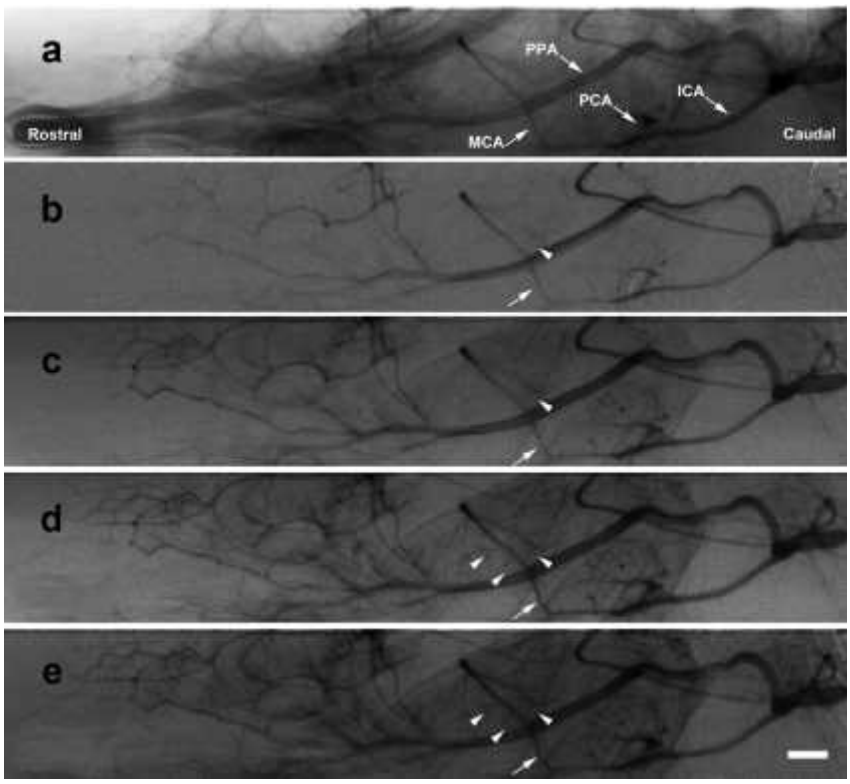

Figure 3. Series microangiography of mouse LSAs. (A) Raw data of cerebral imaging with background noise. (B) This image shows the angiography one second after iodine injection with the bone signal eliminated by background subtraction. The arrow indicates the origin of the MCA. The arrowhead indicates two LSAs that were detected immediately after injection. (C) Two LSAs (arrowheads) derived from the stem trunk of the MCA were represented clearly two seconds after iodine injection. (D) Three seconds after injection the left arrowheads point to the two new emerging LSAs. Note that one originated from the second branch of the stem trunk, while the other arose directly from the stem trunk. (E) Three and a half seconds after injection, all the LSAs were clearly seen on a single image. LSA, lenticulostriate artery; MCA, middle cerebral artery. Exposure time: 20ms, Acquisition rate: 172 ms/image. Scale bar = 1 mm.

the circle of Willis including the internal carotid artery (ICA), anterior cerebral artery (ACA), MCA, and posterior cerebral artery (PCA) were all distinctly detected. Of all the mice we used in this study, we found that only 40% of ICR mice had two posterior communicating arteries (PcomA). The remaining mice had either one or no PcomA, which agrees with the results of a previously reported study on the variations of the ICR mouse PcomA (18).

A series of microangiographs were recorded simultaneously with the injection of the contrast agent nonionic iodine. Contrast agent was injected into the common carotid artery (CCA) at a rate of 33.3 microliter/sec over 3 seconds for a total volume of 100 microliter per mouse. Taking a series of images at fixed time intervals during and after injection, we calculated that the arterial phase is approximately 12 seconds. On average, there are 4 to 5 LSA branches from the root of MCA in each hemisphere (Figure 3). The MCAs have an average diameter of 151±12.7 micrometer while LSAs have an average diameter of 43±6.8 micrometer (Table 1). Based on this data we categorized LSAs into two types: those derive from the stem trunk of the MCA, and those stem from the secondary branches of the MCA.

4.2. CT reconstruction

To further study the morphology of LSAs, we performed CT reconstruction by merging 400 transverse CT slices. Evaluation of these reconstructed images revealed 3 types of LSAs in adult mouse. They are derived from three origins: directly from the stem trunk of the MCA, from the secondary branch of the MCA, or from the circle of Willis (Figure 4). Interestingly, these LSAs formed vascular spirals before entering the striatum. Such anatomical structure may account for the high occurrence of cerebral hemorrhage involving the LSAs. Compared to the cortical branches of the MCA, the LSAs are long and

Table 2. Length of LSA and distance of first LSA from the MCA origin

	a	b	c	d	e	f	e	Mean±SD (n=10)
Distance of 1st LSA from MCA origin (mm)	1.90	1.52	0.39	1.37	1.91	1.91	0.49	1.35±0.59
Length of LSA (mm)	3.42	3.39	2.91	3.13	3.21	2.37	2.15	2.94±0.50

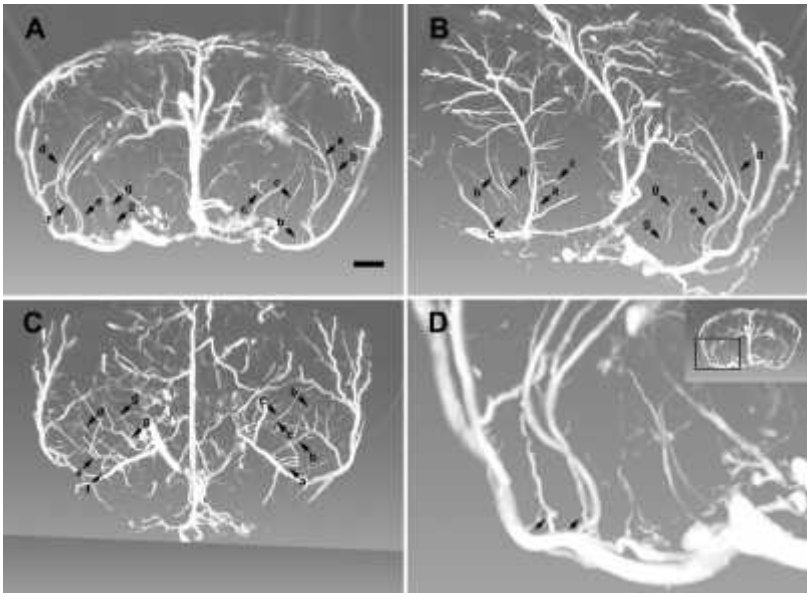

Figure 4. Angiography of forebrain vasculature following imaging reconstruction. (A) In a coronal view of the brain LSAs derived from the MCA stem trunk are indicated by arrows b and e. (B) A sagital view of the brain shows LSAs derived from the secondary branch of MCA, which are indicated by arrows a, d, and f. (C) A superior view of the brain shows LSAs derived from the circle of Willis, which are indicated by arrows c and g. (D) Enlargement of image A. Arrows indicate the spiral pattern of LSAs. LSA, lenticulostriate artery; MCA, middle cerebral artery. Scale bar = 1 mm

thin vessels with few branches (Table 2). Multiple smaller branches and microvessels in the cortex were also detected.

4.3. Ischemia/reperfusion induced hemorrhage due to LSA rupture

Lastly, we examined whether the rupture of LSA is an underlying cause of hemorrhage following transient MCAO by SR microangiography. Mice underwent 1 hour of MCAO followed by 24 hours of reperfusion (17). We detected the leak of contrast agent from LSA and its branches using SR microangiography, which indicates the rupture of LSA and its branches following ischemia/reperfusion (Figure 5). This result suggests that this microangiographic imaging approach could be utilized for the detection of cerebrovascular compromise following ischemia. Moreover, it demonstrates the utility of SR microangiography in elucidating the microvascular pathology underlying ischemia.

5. DISCUSSION

Using the third generation SR microangiography, we report the novel characterization of mouse LSAs *in vivo*. Our findings demonstrate that the LSA may be prone to hemorrhage because of three characteristics: 1.) LSAs have few branches; 2.) they have a tortuous spiral structure that may respond dramatically to hemodynamic changes; and 3.), there is no collateral blood supply (12). Correspondingly, we provide evidence that LSAs are, in fact, prone to hemorrhage following ischemia as demonstrated by the leakage of contrast agent by LSAs in MCAO-treated mice. This technology has far-reaching potential for the study of a number of cerebrovascular-related disorders. Explicitly, it permits the monitoring of the cerebral microvasculature over time, allowing for the delineation of the effects a disease process has on microvasculature and the study of how microvascular changes are associated with disease progression and manifestation.

SR imaging has been developed for about 15 years, and in the past decade it has seen expanding applications in biomedical imaging. A recent report of cerebral angiography using SR observed large vessels including MCA, ACA, PCA, and ICA in mouse brain (19). Other studies using SR imaging include *ex vivo* mouse cerebral angiography using barium sulfate (10, 20), an examination of primate cerebral angiogenesis (21), and *in vivo* imaging of the rat cerebral vascular system (22, 23). Despite these efforts, microangiographic characteristics of the LSA have remained unresolved in living mice. The lack of characterization is likely due to the small size of the LSAs, whose diameter is only about one-fifth of that of the MCA in rats. To our knowledge, this is the first report demonstrating a technology that could accurately detect such small arteries in living mice. Furthermore, our study established a model to study LSA hemorrhage following ischemia.

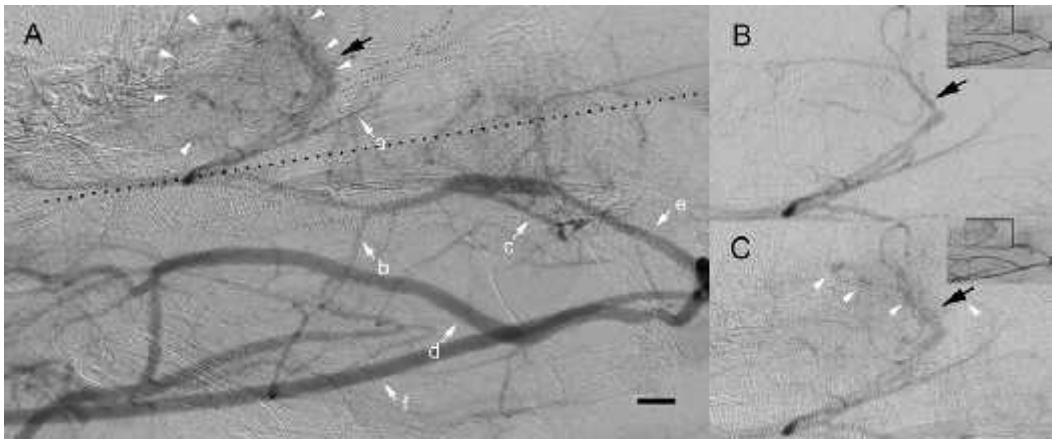

Figure 5. LSA hemorrhage following MCAO. (A) Imaging of the mouse brain was taken three seconds after iodine injection. A dotted straight line is added to provide visual aid for the left (above the line) and right (below the line) hemisphere of the brain. The left ICA is occluded by a nylon suture and therefore it is not visualized in the image. Dotted curve lines were added to illustrate its anatomical position. Arrowheads indicate the hemorrhagic areas in the left brain. There is no hemorrhage in the contralateral hemisphere. The black arrow indicates the MCA in the left hemisphere. (a) ACA; (b) MCA; (c) PCA; (d) PPA; (e) ICA; (f) the PE-10 tube. (B) No visible hemorrhagic leakage is visualized 1.125 seconds after injection. (C) Hemorrhagic leakage is detected 2.25 seconds after injection. White arrowheads indicate hemorrhagic lesion in the LSA territory. LSA, lenticulostriate artery; ACA, anterior cerebral artery; MCA, middle cerebral artery; PCA, posterior cerebral artery; PPA, pterygopalatine artery; ICA, internal carotid artery; and MCAO, middle cerebral artery occlusion. Scale bar = 500 micrometer.

Development of practical techniques to monitor the changes of cerebral vasculature in living animals is a continuous goal of the cerebrovascular research community (24). In this study, we have not only observed the normal cerebral vascular morphology using SR angiography, but also detected the dynamic changes of LSAs. Our data demonstrate that ischemia/reperfusion could induce brain hemorrhage, indicated by contrast agent leakage. Ischemia/reperfusion induced hemorrhage has been reported previously (25, 26). However, previous evidence was obtained from pathological or histological data. In this study, SR microangiography provided direct evidence of hemorrhage *in vivo*, by identifying the branches, the location, and the speed of hemorrhage in the brain in real time. This is important because the LSA branches of the MCA are closely related to hemorrhagic stroke pathology in humans. Overall, this technique thus provides a great potential to further cerebral vascular research in living animals.

SR microangiography can be controlled over a wide range of exposure times and can be reduced to milliseconds. Therefore it has great potential for biomedical application owing to its low radiation dose (27). In our study, a volume of as small as 100 microliter nonionic iodine contrast agent is sufficient to yield clear imaging for the SR angiography.

We performed barium sulfate SR imaging *in situ* initially because raw images with noise of bone and muscle helped to localize ROI of the mouse head in future imaging. During *in vivo* imaging, the animal was positioned so that the arteries of interest could be imaged in a single view window. In addition to cerebral vascular imaging, other vascular systems important in ischemic stroke, such as the ophthalmic arteries, were also clearly observed (Figure 3) (28).

Adult ICR mice were chosen for this study because there are several advantages to using this animal model. For example, many disease models are based on transgenic animals, and transgenic mice are more readily available than other transgenic animals. Mice produce clearer SR images due to less bone-derived noise. Importantly, the field of view (FOV) of the SR angiographic image is relatively narrow making it appropriate for imaging mouse brain since it takes fewer slices to generate an entire image of the brain. Thus, the successful imaging demonstrated in this study provides the proof of principle necessary for further study of cerebral microvasculature in transgenic mouse models.

Safety issues were evaluated for the feasibility of SR imaging. We found that up to one minute of direct synchrotron radiation exposure at 33.2 KeV resulted in no neuronal apoptosis at a one month follow-up (data not shown). The actual exposure time for a single image is about 2 ms. In general, about 100 exposures were applied in one animal, which means that animals received a total of 200 ms exposure time. This exposure duration is much less than standard safety exposure time regulations (29) and therefore this technique could be used for chronic studies.

In conclusion, microscopic cerebral angiography was performed for the first time in living mice by characterizing the three-dimensional morphology of LSAs using state-of-the-art synchrotron radiation. An important application of this technology to the study of cerebrovascular diseases was also established as ischemia-induced hemorrhage of LSAs was detected by SR

microangiography in real time. Overall, SR microangiography is a unique tool with the potential to examine the real time pathology of experimental cerebrovascular diseases in transgenic mice, and it allows for the detection of angiogenesis and vascular integrity, which is useful to evaluate the efficacy of various neuroprotective strategies.

6. ACKNOWLEDGEMENTS

This study was supported by the 973 Program 2010CB834306 (GYY, YW), the Science and Technology Commission of Shanghai Municipality programs 09140902400 and 09ZR1415300 (GYY, YW), and the SMC Excellent Young Faculty Award, A09CX41 (YW). The authors thank Guohao Du and Xiang Gu for their generous technical support.

7. REFERENCES

1. J. Huber: Diabetes, cognitive function, and the blood-brain barrier. *Current pharmaceutical design*, 14 (16), 1594-1600 (2008)

2. S. Achenbach, D. Ropers, M. Regenfus, K. Pohle, T. Giesler, W. Moshage and W. G. Daniel: Noninvasive coronary angiography by magnetic resonance imaging, electron-beam computed tomography, and multislice computed tomography. *Am J Cardiol*, 88 (2), 70-73 (2001)

3. S. Cherry, Y. Shao, R. Silverman, K. Meadors, S. Siegel, A. Chatziioannou, J. Young, W. Jones, J. Moyers and D. Newport: MicroPET: a high resolution PET scanner for imaging small animals. *IEEE Transactions on Nuclear Science*, 44 (3 Part 2), 1161-1166 (1997)

4. S. Takeshita, T. Isshiki, H. Mori, E. Tanaka, K. Eto, Y. Miyazawa, A. Tanaka, Y. Shinozaki, K. Hyodo and M. Ando: Use of synchrotron radiation microangiography to assess development of small collateral arteries in a rat model of hindlimb ischemia. *Circulation*, 95 (4), 805 (1997)

5. H. Mori, K. Hyodo, E. Tanaka, M. Uddin-Mohammed, A. Yamakawa, Y. Shinozaki, H. Nakazawa, Y. Tanaka, T. Sekka and Y. Iwata: Small-vessel radiography *in situ* with monochromatic synchrotron radiation. *Radiology*, 201 (1), 173 (1996)

6. M. Jiang, X. Yang, H. Xu, Z. Zhao and H. Ding: Shanghai Synchrotron Radiation Facility. *Chinese Science Bulletin*, 54 (22), 4171-4181 (2009)

7. D. Cyranoski: China joins world-class synchrotron club. *Nature*, 459 (7243), 16 (2009)

8. H. Yoshino, T. Sakurai, X. S. Oizumi, T. Akisaki, X. Wang, K. Yokono, T. Kondoh, E. Kohmura and K. Umentani: Dilation of perforating arteries in rat brain in response to systemic hypotension is more sensitive and pronounced than that of pial arterioles: simultaneous visualization of perforating and cortical vessels by in-vivo microangiography. *Microvasc Res*, 77 (2), 230-233 (2009)

9. A. Morishita, T. Kondoh, T. Sakurai, M. Ikeda, A. K. Bhattacharjee, S. Nakajima, E. Kohmura, K. Yokono and K. Umetani: Quantification of distension in rat cerebral perforating arteries. *Neuroreport*, 17 (14), 1549-1553 (2006)

10. K. Myojin, A. Taguchi, K. Umetani, K. Fukushima, N. Nishiura, T. Matsuyama, H. Kimura, D. M. Stern, Y. Imai and H. Mori: Visualization of intracerebral arteries by synchrotron radiation microangiography. *AJNR Am J Neuroradiol*, 28 (5), 953-957 (2007)

11. Y. Yamori, R. Horie, H. Handa, M. Sato and M. Fukase: Pathogenetic similarity of strokes in stroke-prone spontaneously hypertensive rats and humans. *Stroke*, 7 (1), 46-53 (1976)

12. L. Bozzao, L. Fantozzi, S. Bastianello, A. Bozzao and C. Fieschi: Early collateral blood supply and late parenchymal brain damage in patients with middle cerebral artery occlusion. *Stroke*, 20 (6), 735 (1989)

13. K. Oka, F. Maehara and M. Tomonaga: Aneurysm of the lenticulostriate artery--report of four cases. *Neurol Med Chir*(Tokyo), 31 (9), 582-585 (1991)

14. A. H. Hainsworth and H. S. Markus: Do *in vivo* experimental models reflect human cerebral small vessel disease? A systematic review.*J Cereb Blood Flow Metab*, 28 (12), 1877-1891 (2008)

15. R. Larrazabal, D. Pelz and J. M. Findlay: Endovascular treatment of a lenticulostriate artery aneurysm with N-butyl cyanoacrylate. *Can J NeurolSci*, 28 (3), 256-259 (2001)

16. M. Komiyama, T. Yasui, K. Tamura, Y. Nagata, Y. Fu and H. Yagura: Simultaneous bleeding from multiple lenticulostriate arteries in hypertensive intracerebralhaemorrhage. *Neuroradiology*, 37 (2), 129-130 (1995)

17. G. Yang, P. H. Chan, J. Chen, E. Carlson, S. F. Chen, P. Weinstein, C. J. Epstein and H. Kamii: Human copper-zinc superoxide dismutase transgenic mice are highly resistant to reperfusion injury after focal cerebral ischemia. *Stroke*, 25 (1), 165-170 (1994)

18. K. Murakami, T. Kondo, M. Kawase and P. H. Chan: The development of a new mouse model of global ischemia: focus on the relationships between ischemia duration, anesthesia, cerebral vasculature, and neuronal injury following global ischemia in mice. *Brain Res*, 780 (2), 304-310 (1998)

19. K. Kidoguchi, M. Tamaki, T. Mizobe, J. Koyama, T. Kondoh, E. Kohmura, T. Sakurai, K. Yokono and K. Umetani: *In vivo* X-ray angiography in the mouse brain using synchrotron radiation. *Stroke*, 37 (7), 1856-1861 (2006)

20. J. Reichold, M. Stampanoni, A. Lena Keller, A. Buck, P. Jenny and B. Weber: Vascular graph model to simulate

the cerebral blood flow in realistic vascular networks. *J Cereb Blood Flow Metab*, 29 (8), 1429-1443 (2009)

21. L. Risser, F. Plouraboué, P. Cloetens and C. Fonta: A 3D-investigation shows that angiogenesis in primate cerebral cortex mainly occurs at capillary level. *International Journal of Developmental Neuroscience*, 27 (2), 185-196 (2009)

22. M. Shirai, D. O. Schwenke, G. A. Eppel, R. G. Evans, A. J. Edgley, H. Tsuchimochi, K. Umetani and J. T. Pearson: Synchrotron-based angiography for investigation of the regulation of vasomotor function in the microcirculation *in vivo*.*ClinExpPharmacolPhysiol*, 36 (1), 107-116 (2009)

23. K. Umetani, K. Kidoguchi, A. Morishita, X. Oizumi, M. Tamaki, H. Yamashita, T. Sakurai and T. Kondoh: *In vivo* cerebral artery microangiography in rat and mouse using synchrotron radiation imaging system.*Proceedings of the 29th Annual International Conference of the IEEE*,France August 23–26 (2007)

24. N. Beckmann, A. Schuler, T. Mueggler, E. P. Meyer, K. H. Wiederhold, M. Staufenbiel and T. Krucker: Age-dependent cerebrovascular abnormalities and blood flow disturbances in APP23 mice modeling Alzheimer's disease. *J Neurosci*, 23 (24), 8453-8459 (2003)

25. L. Latour, D. Kang, M. Ezzeddine, J. Chalela and S. Warach: Early blood-brain barrier disruption in human focal brain ischemia. *Annals of neurology*, 56 (4), 468-477 (2004)

26. H. K. Eltzschig and C. D. Collard: Vascular ischaemia and reperfusion injury. *Br Med Bull*, 70, 71-86 (2004)

27. F. Arfelli, M. Assante, V. Bonvicini, A. Bravin, G. Cantatore, E. Castelli, L. Dalla Palma, M. Di Michiel, R. Longo, A. Olivo, S. Pani, D. Pontoni, P. Poropat, M. Prest, A. Rashevsky, G. Tromba, A. Vacchi, E. Vallazza and F. Zanconati: Low-dose phase contrast x-ray medical imaging. *Phys Med Biol*, 43 (10), 2845-2852 (1998)

28. T. K. Tatemichi, A. Chamorro, G. W. Petty, A. Khandji, L. A. Oropeza, D. I. Duterte and J. P. Mohr: Hemodynamic role of ophthalmic artery collateral in internal carotid artery occlusion. *Neurology*, 40 (3 Pt 1), 461-464 (1990)

29. D. J. Brenner and E. J. Hall: Computed tomography--an increasing source of radiation exposure. *N Engl J Med*, 357 (22), 2277-2284 (2007)

Key Words: Cerebral vasculature, Lenticulostriate artery, Microangiography, Mouse, Synchrotron radiation

Send correspondence to: Guo-Yuan Yang, Neuroscience and Neuroengineering Center, Med-X Research Institute, School of Biomedical Engineering, Shanghai Jiao Tong University, 1954 Hua-shan Rd, Shanghai 200030, China, Tel: 86-21-62933186, Fax: 86-21-62932302, E-mail: gyyang0626@gmail.com